Structural Changes during Plastic Deformation at Crack Tips in PVDF Films: A Scanning X-ray Scattering Study

Günther A. Maier,[†] Gernot Wallner,[‡] Reinhold W. Lang,[‡] and Peter Fratzl*[,§]

Material Center Leoben, Erich Schmid Institute of Material Science, and Institute of Metal Physics, University of Leoben, Leoben, Austria; Polymer Competence Center Leoben and Institute of Materials Science and Testing of Plastics, University of Leoben, Leoben, Austria; and Department of Biomaterials, Max Planck Institute of Colloids and Interfaces, 14424 Potsdam, Germany

Received February 23, 2005; Revised Manuscript Received May 12, 2005

ABSTRACT: The fracture behavior of semicrystalline polymers is controlled by the micromechanisms associated with formation and breakdown of a plastic deformation region at notches, cracks, or other stress raising defects. In this context, it is widely acknowledged that material toughness may arise from the volume of the plastically deformed crack tip region along with energy dissipating structural changes of the material within this region. In general, a wide variety of such structural mechanisms are concernable, and little is known so far on specific details. Recently, scanning small- and wide-angle X-ray scattering approaches with positional resolution in the micron range have demonstrated to make such structural information at the supramolecular level accessible. This methodology was used in the present investigation to study the plastic deformation-induced structural changes ahead and around crack tips in a film of poly(vinylidene fluoride) (PVDF). The PVDF investigated exhibited a crystalline morphology of the α-form in the initial state. The micromechanisms of cavitation and fibril formation in highly stretched double-edge notched tensile specimens were elucidated for the mid-rib and outer plastic zone in a position resolved manner. Of particular importance, a phase transformation from a α-to-β morphology was detected at room temperature in the crack tip plastic deformation zone, depending on the position and distance relative to the crack tip. The various features of the plastic deformation process (cavities, fibril diameters, main fibril orientations, α-to-β-phase ratios) were analyzed and assessed semiquantitatively.

Introduction

Semicrystalline polymers are hierarchically structured materials, and they usually show a complex fracture behavior, preceded by numerous plastic deformation mechanisms related to the formation of crazes and shear zones at notches or cracks or other stress raising defects. The micromechanisms in the case of crazing include the nucleation and subsequent growth of microvoids along with the formation a fibril network and in the case of shear yielding the nucleation and growth of shear bands. In numerous semicrystalline plastics both mechanisms were found to occur simultaneously on a local scale when irreversible deformations are applied. Moreover, both crazing and shear yielding represent plastic deformation modes with high molecular orientations, which in the case of semicrystalline plastics may result in a phase transformation (breakdown of lamellar and spherulitic structures and subsequent recrystallization). In addition, crazing involves the formation of voids, thus representing also a density inhomogeneity.[1−3] Despite their importance in controlling crack growth resistance and fracture toughness, the details of the underlying processes of void formation and growth, molecular orientation, and phase transformation in these crack tip plastic deformation zones are as of now only poorly understood. So far, any structural changes occurring during plastic crack tip deformation in semicrystalline plastics have been mostly characterized using light and electron microscopy.[4−6] The difficulty with transmission electron microscopy techniques is related to specimen preparation and to the efforts required to obtain statistically relevant, quantitative structural parameters. Other widely used methods to determine structural properties, describing lamellar spacing, phase composition, texture, size, and orientation of defects, are small- and wide-angle scattering of X-rays (SAXS and WAXS) or neutrons.[7−15] However, because of the extreme deformation gradient close to the crack tip, scattering methods will only provide a significant information, if used in a position-resolved manner. The spatial resolution should be adapted to the size of the deformation zone, which requires a beam diameter in the range of a hundred micrometers or less. Position-resolved experiments of this type have been performed up to now in several materials, such as metals,[16] PMMA−PMMA interfaces,[17] and polystyrene,[18] for crazing,[9] and in biological tissues like wood or bone,[19,20] often using synchrotron radiation.

In this paper, we used scanning-SAXS and -WAXS to study the deformation zone near the crack tip in poly(vinylidene fluoride) (PVDF) specimens of the double-edge notched tension (DENT) type. PVDF is a semicrystalline thermoplastic polymer exhibiting at least four polymorphous states, referred to as α, β, γ, and δ. The different crystalline morphologies allow a broad range of properties and applications. In particular, the α-form is used in a variety of applications requiring specific optical, chemical, or electrical requirements. The β-form exhibits ferroelectric properties which are useful, e.g., for sensors. A potential new field of applications

[†] Material Center Leoben, Erich Schmid Institute of Material Science, and Institute of Metal Physics, University of Leoben.
[‡] Polymer Competence Center Leoben and Institute of Materials Science and Testing of Plastics, University of Leoben.
[§] Max Planck Institute of Colloids and Interfaces.
* Corresponding author: e-mail Peter.Fratzl@mpikg.mpg.de; Fax +49 331 567 9402.

10.1021/ma050390f CCC: $30.25
Published on Web 06/17/2005

Table 1. Orthorhombic Lattice Parameters of α- and *β*-PVDF[22]

	a (Å)	*b* (Å)	*c* (Å)
α-PVDF	4.96	9.64	4.62
β-PVDF	8.58	4.91	2.56

for PVDF is in solar energy devices. For example, nonpolar α-PVDF encapsulation films are currently investigated for photovoltaic modules, which are multilayer components of flexible and stiff materials.[21]

In terms of crystal cell structure, both α and *β* modifications are orthorhombic with lattice spacing values given in Table 1. The different phases and their properties have been reviewed by Lovinger[22] and Keppler and Anderson.[23]

From the different crystal modifications, the nonpolar α-form is most commonly observed and obtained when the material is solidified from the melt by simple cooling procedures. The polar *β*-form is obtained by other routes, either directly from the melt[24] or by deformation-induced phase transformation from the α-modification. This α-to-*β* transformation has been investigated by many researchers[25−27] in the context of the specific electrical and ferroelectric properties of the *β*-phase.

The mechanical and micromechanical properties of α-PVDF and mixtures of α- and *β*-PVDF have been investigated in slabs of PVDF[28,29] and in fibers[13] using tensile tests at different temperatures and deformation rates. In these studies valuable insight was gained about the α-to-*β*-phase transformation, cavitation, and fibrillation in PVDF depending on the test method. In all cases the formation of microvoids and cavities in the initial stages of the plastic deformation process was detected. At high deformation speeds and low temperatures cavitation was observed to be dominant, while at high temperatures and low deformation rates shear yielding was determined to be the main deformation mechanism with a negligible or no role of cavitation. Interestingly, as of now no study is available investigating the detailed mechanisms of crack tip plastic zone formation in α-PVDF.

The present study was done to gain a comprehensive understanding of the morphological and structural details of the crack tip plastic zone formation process in α-PVDF. This was done by generating complete scattering maps of the plastic deformation zone in the region of the unbroken ligament of doubled notched specimens of a PVDF film tested in tension. On the basis of the results, a model is proposed for the various plastic deformation processes occurring ahead of the crack tip and in the unbroken ligament in α-PVDF prior to crack propagation.

Experimental Section

Material and Specimen Preparation. The 200 *μ*m thick α-PVDF films with a melting peak temperature of 170 °C studied in this paper were supplied by Solvay Advanced Polymers France S.A (Paris-Cedex, F). The films were produced by the supplier on a lab-scale extruder. The molecular mass distribution, determined by SEC using poly(methyl methacrylate) standards (PMMA), is characterized with values for $\bar{M}_n$ = 150 050 g/mol and for $\bar{M}_w$ = 278 500 g/mol. Fourier transform infrared spectroscopy (FTIR) revealed a small amount of chain defects (head-to-head and tail-to-tail connections).

From the 200 *μ*m thick films, rectangular samples having a width of 30 mm and a length of 120 mm were cut parallel to the extrusion direction. The visually transparent films were razor notched to obtain double-notched tensile specimens, with an unbroken ligament length of 12 mm and symmetrical initial razor notches. The notching did not lead to a visible stress whitening of the material, even close to the crack tip. Tensile tests were performed at 23 °C and 50% relative humidity at a displacement rate of 1 mm/min using a screw-driven tensile test system (model 4505, Instron Limited, High Wycombe, UK) with a 1 kN load cell. The DENT specimen was deformed up to a point at which the plastic deformation zone covered the entire unbroken ligament, and the cracks from both sides at the notch tips had propagated 1−2 mm. At this stage of deformation, it is very unlikely that the initial notching had any influence on the plastic zone in between the two crack tips. The test was stopped, and the sample was unloaded by fast opening of the clamps in the tensile testing machine. These samples were used for scanning-WAXS and -SAXS experiments as well as for additional characterization in the scanning electron microscope (Leo 1525). For the SEM measurements, the sample was sputtered with a thin film of gold.

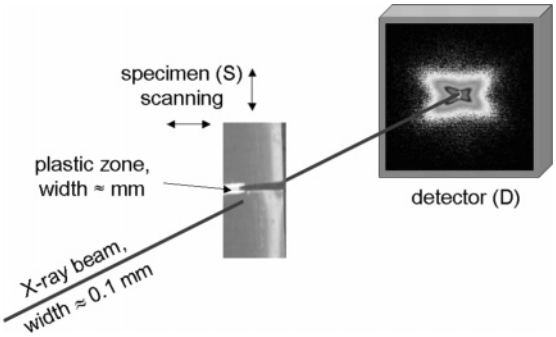

Figure 1. Sketch of the measuring setup. The specimen (S) was mounted on a XY stage which could be moved with an accuracy of 2 *μ*m. The plastic zone and the surrounding area were scanned with a beam with ≈0.1 mm in diameter. The detector (D) was moved to distances of ∼6 cm (WAXS mode) and ∼64 cm (SAXS mode) to the sample.

X-ray Scattering Experiments. For the X-ray measurements, the unloaded samples were fixed on the sample holder of the instrument. The scanning-WAXS and -SAXS measurements were carried out on a pinhole SAXS camera (NanoSTAR, Bruker AXS; Karlsruhe, D) in transmission mode with X-rays from a rotating anode generator providing a radiation with a wavelength of 1.54 Å (Cu Kα). The sample holder allowed a controlled movement of the sample within the instrument in the $x-y$ plane perpendicular to the X-ray beam, which had a diameter of ≈0.1 mm (Figure 1). The NanoSTAR instrument was equipped with a 2D position-sensitive detector which could be placed in different distances from the sample, allowing to perform SAXS and WAXS measurements with the same device. The sample-to-detector distance for the SAXS measurements was 64 cm and for the WAXS measurements 6 cm. The distance between sample and detector was calibrated using an Ag-behenate reference sample for the SAXS setup and corund for the WAXS setup. One-half of the DENT specimen was chosen to perform the scanning-SAXS and -WAXS experiments with a measuring grid of 0.2 × 0.2 mm^2.

The measuring protocol was as follows: In a first step in the SAXS mode, a radiography of the specimen was taken. The radiography was obtained by measuring the transmission of the specimen every 200 *μ*m with an X-ray-sensitive diode placed into the beam directly after the sample. The diode signal was proportional to the intensity of the X-ray beam transmitted through the specimen. A specially designed software[19] displayed the radiography of the sample and was used to select the measuring positions on it. Around the crack tip an area of 3 × 1.8 mm^2 was scanned in steps of 0.2 mm in both directions. For the WAXS measurements, the sample had to be fixed on an additional sample holder, allowing to shorten the sample-to-detector distance down to 6 cm. Position marks on the sample holder ensured that similar measuring positions for both SAXS and WAXS were chosen. For the data interpretation and evaluation all scattering patterns were corrected for background scatter.

Scanning-SAXS Data Analysis. For the determination of morphological parameters, isotropic SAXS patterns $I(q,\psi)$ were radially averaged with respect to ψ, yielding the $I(q)$ scattering curves, q being the scattering vector. They were analyzed applying a 1D correlation function method[30,31] to calculate the long period and the thickness of the crystal lamellae. Oriented SAXS patterns were reduced by averaging within arcs from $\psi = -15$ to 15, where the main direction of the oriented signal was defined as $\psi = 0$. For fibril-like structures, a cross-sectional radius of gyration R_{gc} was derived using an exponential law, modified from the usual the Guinier law:[32,33]

$$qI(q) = I_1 \exp(-q^2 R_{gc}^2/2) \quad (1)$$

where I_1 is the limit value of $qI(q)$ for $q \to 0$. Assuming a circular cross section of the rod, the radius of the circle R_c is equivalent to $\sqrt{2}R_{gc}$. This procedure allowed the determination of the mean fibril diameter without a knowledge of their volume fraction, which would be needed for the more rigorous methods proposed, e.g., by Salomons et al.[34] For platelike structures, we used a second type of modified Guinier law:

$$q^2 I(q) = I_2 \exp(-q^2 R_{g1}^2) \quad (2)$$

where I_2 is the limit value of $q^2I(q)$ for $q \to 0$. R_{g1} is the one-dimensional "radius of gyration", simply given by $R_{g1} = D/\sqrt{12}$, where D is the height of the plates. Clearly, the Guinier laws (1) and (2) are valid only under the assumption of a sufficiently large distance between the fibers or cracks[32,33] (low-density limit). We used the Guinier approximation in the q range, where $qR_{gc} < 1$, corresponding roughly to its typical range of validity.[32,33]

To image and quantify the predominant orientation of the structures within the sample at different measuring points, the q averages from $I(q,\psi)$ were computed, yielding a function $I(\psi)$ of the polar angle ψ. Peaks in the $I(\psi)$ curve yield directly the predominant orientation of the structure elements rotated by 90°.

Scanning-WAXS Data Analysis. The WAXS patterns have been used to investigate phase compositions of the sample. The amount of different crystalline phases in a sample is directly related to the integral scattering intensity of the contributions from each phase. In the case of tested PVDF samples the mass fraction of the β-phase (X_β) could be estimated using following considerations: The α-phase has the reflections $(100)^\alpha$, $(020)^\alpha$, and $(110)^\alpha$ in the region between $2\theta = 15-22°$, 2θ being the scattering angle. In this area also the $(100)^\beta$ and $(200)^\beta$ reflections appear. To distinguish between α and β, we turn to the region $2\theta = 23-27°$, where the $(021)^\alpha$ and $(120)^\alpha$ reflections do not overlap with contributions from the β-phase. A parameter ρ^α was first calculated from the WAXS signal of undeformed (and isotropic) α-phase by the ratio

$$\rho^\alpha = \frac{I^\alpha_{100} + I^\alpha_{020} + I^\alpha_{110}}{I^\alpha_{021} + I^\alpha_{120}}$$

I^α_{100} and other similar expressions represent the integrated peak intensities. Calculating a similar intensity ratio for an $\alpha-\beta$ mixture, one obtains

$$\rho^{\alpha+\beta} = \frac{I^\alpha_{100} + I^\alpha_{020} + I^\alpha_{110} + I^\beta_{012} + I^\beta_{120}}{I^\alpha_{021} + I^\alpha_{120}}$$

A rough estimate of the α/β-phase ratio was obtained by the difference $\rho^{\alpha+\beta} - \rho^\alpha$, which is proportional to this phase ratio. As the proportionality constant is unknown, only relative changes in β content may be assessed.

Results

The typical load−displacement curve of the investigated double-notched α-PVDF film is shown in Figure 2 along with pictures illustrating the double-notched region of the deformed specimen for various deformation stages. In the first region of the load−displacement diagram plastic deformation zones with a white appearance develop at both razor notch tips. As the load is increased to the maximum point, the plastic deformation zones growing from both notch tip sides approach one another and coincide. This causes the load deformation instability in the region immediately following the load maximum and leads to a state of full ligament yielding. Upon further deformation, crack growth from the meanwhile blunted razor notch roots commences and a transparent mid-rib region surrounded by an outer white region develops in the unbroken ligament plastic zone. This process of crack growth continues until ultimate failure and specimen separation occurs.

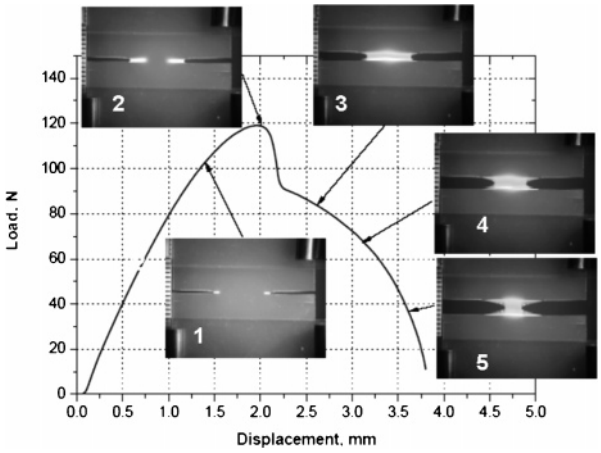

Figure 2. Typical load−displacement curve of the investigated DENT PVDF sample with a width of 30 mm and a ligament length of 12 mm; the micrographs illustrate the specimen appearance at various deformation levels. The white regions ahead of the notch tips and in the unbroken ligament indicate the extent of plastic deformation.

For the scanning-X-ray scattering investigations a specimen was used which was deformed to a point corresponding to position 3 in Figure 2. The sample was unloaded by opening the clamps and had a remaining ligament length of ≈9 mm. The scanned area was chosen to be big enough to cover the whole deformation zone around one crack tip and had an extension of 3 mm in the crack propagation direction and 1.8 mm in height.

Figure 3 shows the original 2D-SAXS patterns in a composite picture and reveals significant differences in the scattering patterns depending on the position while exhibiting a high symmetry of the structure with respect to a horizontal plane, i.e., the crack plane. According to the shape of the scattering patterns, the scanned area could be subdivided into several areas with different microstructure: (i) the undeformed area, far away from the crack tip (for example point 1); (ii) the outer plastic deformation zone (marked as 2); (iii) the most heavily deformed area of the mid-rib plastic zone (indicated with (3,4,5)). Looking at Figure 3 from the bottom upward, the first line of SAXS patterns just show rings, for example point 1. These rings are due to the lamella structure of the native α-PVDF material. Going upward to the next line of scattering patterns, for example point 2, a second element emerges in the SAXS patterns, two points oriented in line with the deformation axis. The ring from lamellae scattering is still visible, and the two points are most likely due to defects in the material.

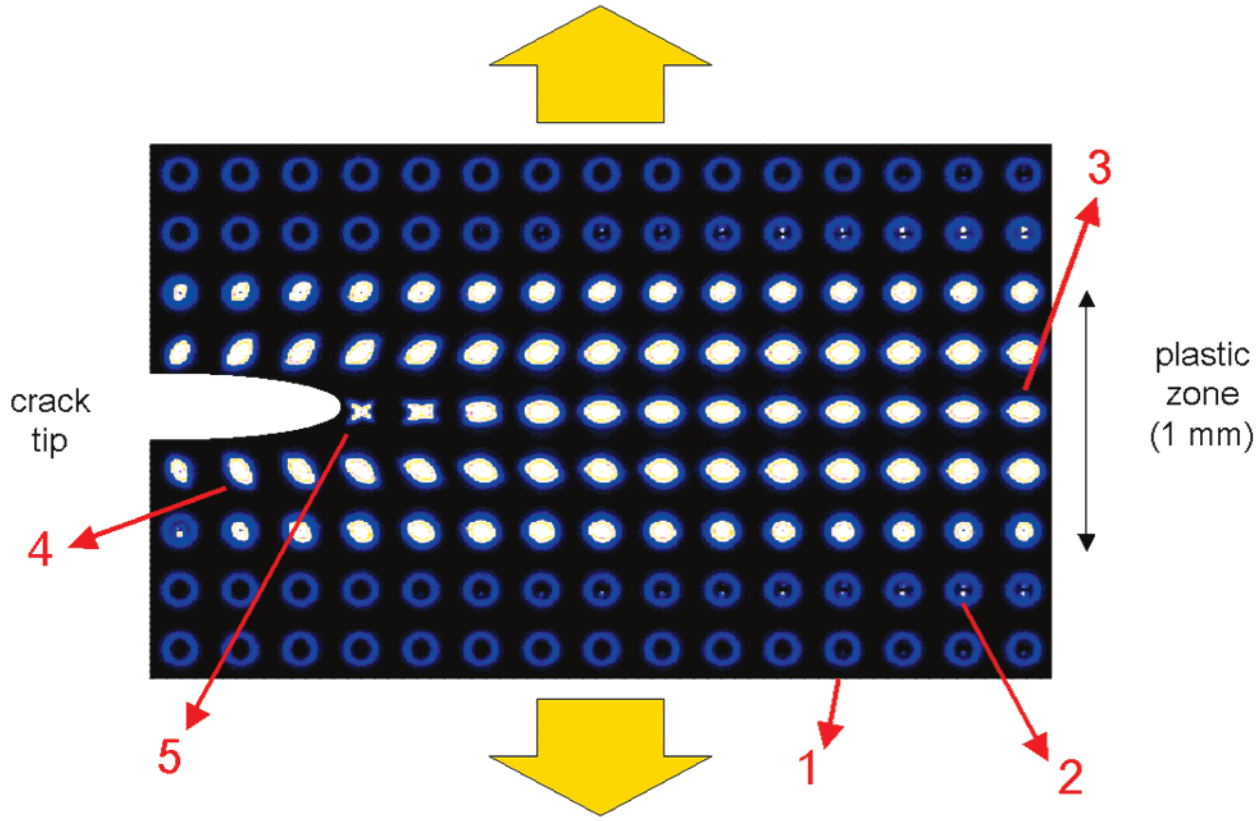

Figure 3. SAXS patterns from the crack tip and the surrounding area of the unbroken ligament. The arrows denote the deformation direction. Each SAXS pattern corresponds to a beam size of ≈0.1 mm and is positioned in the center of a squared area element of 0.2 × 0.2 mm^2. The plastic zone dimension in the direction of deformation was about 1.4 mm in height and covers the entire unbroken ligament of the specimen. The patterns show isotropic scattering (rings) in the undeformed area far away from the crack tip (1), isotropic and a second signal orientated parallel to the deformation axis (2), oriented scatter (3,4), and finally crosses just ahead of the crack tip (5).

Moving toward the center in Figure 3, the SAXS patterns change dramatically. Looking at position 3, one notices that there are no circular rings, but elliptical patterns. The ellipse is oriented orthogonal to the deformation axis far away from the crack tip. At position 4, located in the wake of the crack tip, the ellipse is tilted 30° from the strain axis. The tilt angle of the patterns in this plane is increasing along the crack propagation direction. Very near the crack tip, crosses can be seen on the patterns, numbered with 5 in Figure 3, which indicate the superposition of two structural elements with different orientation.

In Figure 4, selected SAXS and corresponding WAXS patterns for positions indicated in Figure 3 and using the same number codes are shown in more detail. In the undeformed area (position 1) both the SAXS and WAXS patterns show isotropic scattering, and the scattering signals can be described as rings. In the WAXS pattern, four rings are visible, and all can be regarded as belonging to the α-phase of the PVDF crystals. While WAXS probes the crystallographic composition and texture, SAXS is sensitive to the morphology, like lamellae distribution, microvoids, cracks, and fibrils. Therefore, the isotropic ring in the SAXS patterns corresponds to an isotropic distribution of lamellae orientations, probably due to the spherulitic structure of the material.

At position 2, located at the edge of the plastic zone, a second contribution in the SAXS pattern is visible, a vertical streak in the center. The isotropic scatter from the lamellae is still visible, indicating that there were no changes in the overall lamellae morphology. The streak in the center of the SAXS pattern could arise from cavities in the material, oriented orthogonal to the tensile direction. This explanation is supported by the high scattering power of the streak in relation to the crystalline−amorphous scatter in the native sample, indicating that electron density contrast provoking this signal was much higher. In addition, no changes in crystal structure are visible in the WAXS patterns at this stage of deformation. In the mid-rib plastic zone far away from the crack tip (position 3) the SAXS pattern is dominated by a broad streak and the ring from lamellae scatter has disappeared. The orientation of this streak or ellipse is orthogonal to the tensile direction. In the WAXS pattern, an oriented signal is also visible. There are still rings from the α-phase, but additional reflections from the β-phase appeared. Only the contribution from β-phase showed a strong orientation in the WAXS pattern. In the plastic zone in the wake of the crack tip (position 4) the SAXS and WAXS patterns show a different orientation of fibril-like structures. In particular, the streak in the SAXS pattern is tilted toward the deformation axis. In the WAXS pattern, rings and peaks are visible. Finally, the SAXS pattern taken from the zone just ahead of the crack tip (position 5) shows two streaks crossing each other, and the corresponding WAXS pattern exhibits four main peaks. The rings are no longer visible.

Quantitative results were obtained from the scattering curves, as exemplified in Figure 5. The Lorenz-corrected SAXS scattering curve and the corresponding 1D correlation function are show in Figure 5a. From the correlation function, the long period and the lamellae

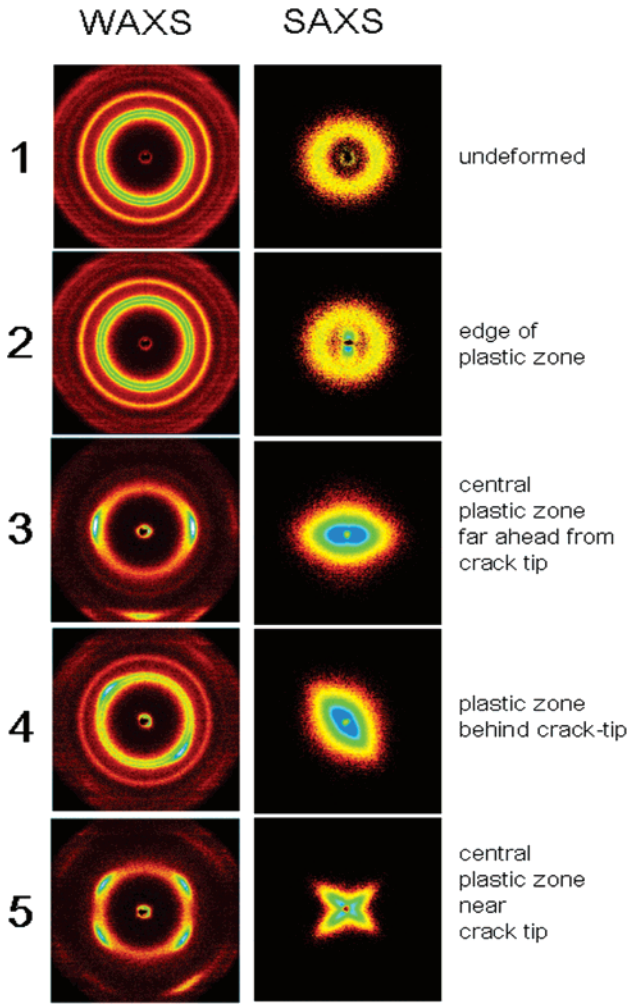

Figure 4. WAXS and the corresponding SAXS patterns from different positions on the sample as marked by numbers in Figure 3. In the undeformed area (1) both the WAXS and the SAXS pattern show isotropic scattering (rings). At the edge of the plastic zone (2), an additional contribution, a vertical streak, raised in the center of the SAXS pattern, while the WAXS pattern kept its rings. In the central zone ahead of the crack tip (3), the SAXS pattern changed to a horizontally oriented elliptic streak, while the WAXS pattern mainly consists of rings and two points in the equator of the pattern. In the plastic zone in the wake of the crack tip (4) the orientation of the elliptic pattern and the two points is tilted about 60°. The central zone near the crack tip (5) shows crossed streaks in the SAXS pattern and four points in the WAXS pattern.

thickness were determined to be 10.5 and 3 nm, respectively, for the undeformed α-PVDF (position 1 in Figures 3 and 4).

Figure 5b shows the scattering curve from the cavities at the edge of the outer plastic zone (position 2 in Figures 3 and 4) and the corresponding modified Guinier plot (based on eq 2). From this plot, the height of the lens-shaped cavities oriented perpendicular to the tensile direction was determined to be approximately 7 ± 1 nm; the extension in the crack plane direction was more than 100 nm. In Figure 5c, scattering curves from positions 3 and 5 of Figures 3 and 4 are shown. From the modified Guinier plot (based on eq 1) the diameter of the fibrils was determined to be 11.5 ± 1 nm just ahead of the crack tip (position 5) and 15 ± 1 nm in the plastic zone mid-rib region far ahead of the crack tip (position 3). Figure 5d shows WAXS curves, taken in the native area of the sample (position 1) and just ahead of the crack tip (position 5). The curves clearly show a change in the diffraction around $2\theta = 18°$, indicating a partial phase transformation from α to β. While in the undeformed native region, the scatter of the α-phase was dominant, the highly deformed crack tip area consisted mainly of the β-phase.

Discussion

In the undeformed area, isotropic scattering arising from the spherulitic structure of α-PVDF was found to be dominant. The long period and lamella thickness were determined to be 10.5 and 3 nm, respectively. Both dimensions did not change significantly within the native area. The beginning of plastic deformation in the transition region toward the outer plastic zone was characterized by the formation of cavities, with roughly planar geometry oriented perpendicular to the tensile direction; the height of the cavities was determined to be about 7 nm and the width above 100 nm. As the specimen was in an unloaded (relaxed) state, the height dimension in the loaded state would be probably significantly higher. The scattering results revealed that the formation of cavities occurred without a significant structure change of the original polymer morphology. In other words, in this region crystal lamella and spherulites have not yet been changed by deformation. On the other hand, for the mid-rib plastic zone region, scattering patterns indicated significant structural changes. The original spherulitic material had disappeared completely and was replaced by material consisting of highly oriented fibrils embedded in a low-density matrix of α-PVDF. While the fibrils far away of the crack tip are oriented mainly in the deformation direction, they are tilted under certain angles in the region surrounding the crack tip. Just ahead of the crack tip the fibrils appear to form a cross-plied structure. Simultaneously, a phase transformation from α- to β-PVDF occurred, leading to the conclusion that the fibrous material is formed by β-PVDF. This is supported by the fact that the crystalline reflections from β-PVDF are oriented in the same direction as the fibrils (Figure 4, positions 3−5), while the remaining α-PVDF phase stayed fully isotropic. Moreover, in the heavily deformed zone ahead of the crack tip (position 5 in Figure 5), almost no α-PVDF remains, and only fibrils with β-PVDF were detected. In this context, it is well-known that in PVDF stress induced α-to-β-phase transformation takes place.[13,26−28] Moreover, phase transformations at crack tips has also been reported as important toughness enhancing mechanism for semicrystalline poly(propylene) (PP).[35]

The distribution of the β-phase within the sample, determined by WAXS, corresponded strongly to the amount of fibrous material. In Figure 6a the β/α ratio at different positions of the sample is shown. In the transitional region from the native material state to the outer plastic zone, where the cavities were formed, no phase transformation was found to occur. Figure 6b shows a light microscopy picture of the crack tip region; the main direction of the well-oriented fibrous structures (as determined by SAXS) is also indicated in the micrograph. There is a slight asymmetry between the top and the bottom in Figure 5, arising from a tilt of the sample in the holder of the SAXS instrument.

It is interesting to note that the fibril direction in Figure 6b mirrors the main shear directions in the material according to the slip line theory.[36] This theory

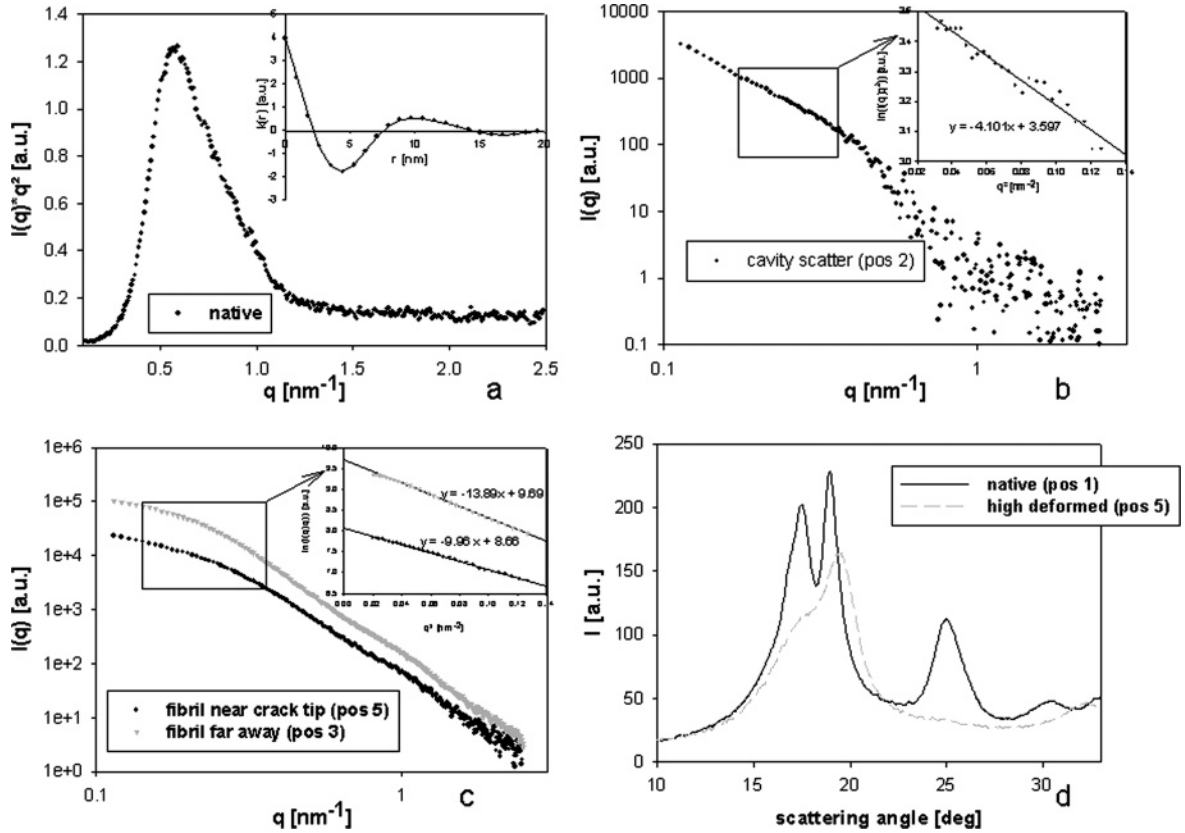

Figure 5. Scattering curves from different positions of the DENT specimen (number codes for the position are indicated in Figure 3): (a) Lorenz-corrected SAXS curve and its corresponding 1D correlation function from the native sample (position 1), (b) SAXS curve and Guinier plot from position 2, (c) SAXS curves from fibrils at positions 3 and 5 and corresponding Guinier plot, and (d) WAXS curves from the native and the highly deformed crack tip area (positions 1 and 5).

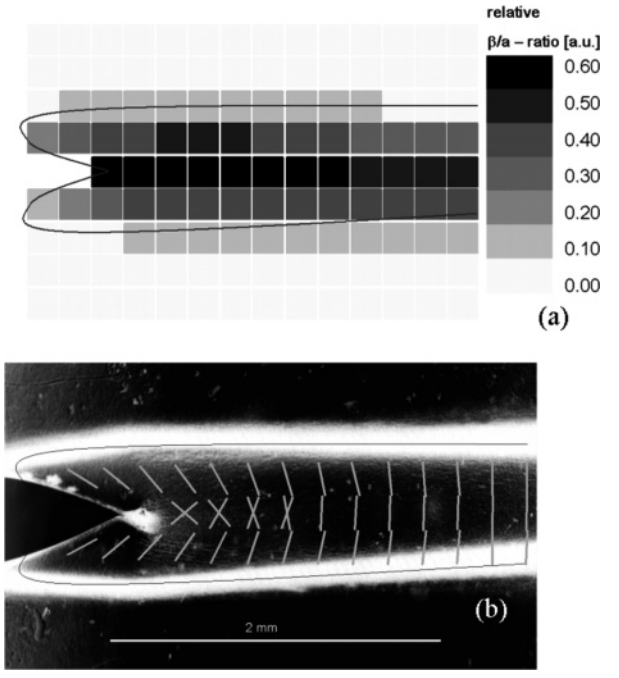

Figure 6. Distribution of the β-phase around the crack tip and orientation of the fibrous structures. (a) shows the β/α ratio around the crack tip, as calculated from WAXS measurements. The tin line indicates the border of the deformation zone, which can be seen in (b) as a bright line. (b) shows a micrograph of the sample; the fibril direction, derived from SAXS, is indicated by straight lines.

describes in principle the plain shear deformation of perfectly plastic materials, with the maximum resolved shear stress in the plane of deformation having a constant volume during plastic flow. This assumption should be accurate for DENT polymer samples as used in this study. The effect of crack tip blunting on the geometry of the slip line field in near tip region[37] leads to the formation of crossed shear directions. The opening angle between the theoretical main shear lines is decreasing with distance from the tip. This effect can clearly be seen in Figure 6b. The diameter of the fibrils also changed with respect to the position within the sample. In the central area far ahead from the crack tip the mean diameter was determined to be 15 ± 1 nm and directly at the crack tip 12 ± 1 nm.

A summary of the processes accruing ahead of the crack tip in α-PVDF is sketched in Figure 7. In a region, far away from the crack tip, elongated cavities were formed. The orientation of the cavities was perpendicular to the strain axis. In this area, neither a change in the long period or in the orientation of lamellae nor a phase transformation occurred. This indicated that the cavities were formed between the lamellae stacks, as proposed by Castagnet et al.[38] Closer to the crack tip, crazes were formed, and simultaneously, a partial phase transition from α to β occurred. The remaining α-PVDF kept its isotropic character, while the β-form was highly orientated, forming fibrils. These were oriented parallel to the direction of the highest shear stresses within the sample. Therefore, mapping the directions of the fibrils is roughly equivalent mapping the mean shear stress direction in the sample. Directly at the crack tip, a very strong fibrillation of the material occurred, corresponding to formation of fibrils separated by microvoids. The β/α ratio increased when the fibrous structures became

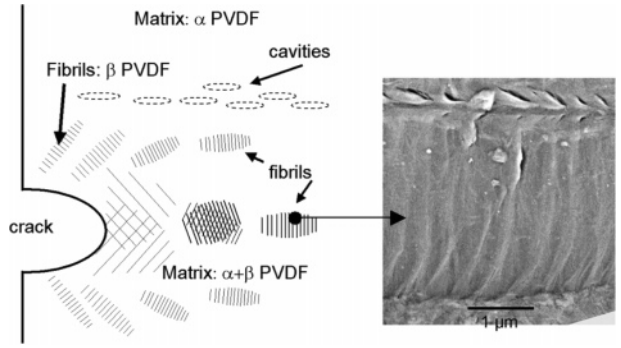

Figure 7. Sketch of the deformation and main features within the sample. Cavities are drawn with dotted lines and fibrous structures as lines. The content on β-PVDF was directly connected to the amount of fibrillar material. The arrow denotes the position where the corresponding SEM micrograph was taken (position 3 in Figures 3 and 4). The micrograph shows the fibrillous morphology of sample in the highly deformed area.

more and more dominant. At the crack tip, a nearly complete transition from α to β-PVDF had occurred.

The fracture of α-PVDF is controlled by different mechanisms; the material has various possibilities to dissipate energy and, hence, for increasing the toughness. The influence of the morphology on the strength of the material can be described as follows: The formation of a big plastic zone, characterized by cavitation, dissipates much energy within the material. These cavities lead to stress whitening as shown in Figure 2. At this stage, a significant load drop can be seen in the load−extension curve (Figure 2). This load drop corresponds to the beginning of fibrillation associated with a phase transformation from α- to β-PVDF in the fibrils. The new α- and β-PVDF matrix forms the crack progression zone, allowing continuous crack propagation to the final breakdown of the material. The final toughening mechanism of the material is the stretching and thinning of the β-fibers before the crack propagates.

Conclusion

The results show clearly the potential of position-resolved scattering methods in studying fracture processes in polymers. Morphological changes could be detected near crack tips in α-PVDF tested in tension as DENT samples, and a model for crack propagation was proposed: The fracture of this material starts by the formation of cavities oriented orthogonal to the strain axis and large enough to scatter light. Moreover, a partial phase transformation from α- to β-PVDF occurs in the plastic process zone. Most interestingly, the β-phase appears in fibrils oriented along the main shear directions within the sample, as predicted by the slip line theory. This β-fibrils are the further strained until failure of the material, which seems to be controlled by the behavior of these very thin β-PVDF fibers. During the progression of the crack, a range of phenomena is observed, all of them reducing the stress in the matrix ahead of the crack tip. There is the formation of cavities, fibrillation, and phase transformation, which all help to dissipate energy and, hence, increase the toughness of the material.

Acknowledgment. The research work in the Materials Center Leoben (MCL) and in the Polymer Competence Center Leoben (PCCL) was supported by the Kplus-program of the Austrian Ministry of Traffic, Innovation and Technology and by Bruker AXS, Karlsruhe, Germany. The PCCL is also supported by the State Governments of Styria and Upper Austria.

References and Notes

(1) Kausch, H.-H. *Polymer Fracture,* 2nd ed.; Springer: New York, 1987.
(2) Grellmann, W. *Deformation and Fracture Behavior of Polymers*; Springer: Berlin, 2001.
(3) Michler, G. H. *Kunstoff-Mikromechanik*; Hanser: München, Wien, 1992.
(4) Michler, G. H.; Godehardt, R. *Cryst. Res. Technol.* **2000**, *35*, 863−875.
(5) Plummer, C. J. G.; Goldberg, A.; Ghanem, A. *Polymer* **2001**, *42*, 9551−9564.
(6) Bretz, P. E.; Hertzberg, R. W.; Manson, J. A. *Polymer* **1981**, *22*, 1272−1278.
(7) Brown, H. R.; Kramer, E. J. *J. Macromol. Sci., Phys. B* **1981**, *19*, 487−522.
(8) Balta-Calleja, F. J.; Vonk, C. G. *X-ray Scattering of Synthetic Polymers*; Elsevier: Amsterdam, 1989.
(9) Legrand, D. G.; Forth, C. M. *J. Polym. Sci., Polym. Lett. Ed.* **1983**, *21*, 853−858.
(10) Fairclough, J. P.; Hamley, I. W.; Terrill, N. J. *Radiat. Phys. Chem.* **1999**, *56*, 159−173.
(11) Butler, M. F.; Donald, A. M.; Ryan, A. J. *Polymer* **1997**, *39*, 781−792.
(12) Stribeck, N.; Buchner, S. *J. Appl. Crystallogr.* **1997**, *30*, 722−726.
(13) Wu, J.; Schulz, J. M.; Yeh, F.; Hsiao, B. S.; Chu, B. *Macromolecules* **2000**, *33*, 1765−1777.
(14) Fratzl, P. *J. Appl. Crystallogr.* **2003**, *36*, 397−404.
(15) Falcao, A. N.; Skov Pedersen, J.; Mortensen, K. *J. Mol. Struct.* **1996**, *383*, 69−74.
(16) Grosse, M.; Boehmer, J.; Riekel, C. *J. Mater. Sci., Lett.* **1998**, *17*, 1631−1634.
(17) Lorenz-Haas, C.; Muller-Buschbaum, P.; Wunnicke, O.; Cassignol, C.; Burghammer, M.; Riekel, C.; Stamm, M. *Langmuir* **2003**, *19*, 3056−3061.
(18) Roth, S.; Burghammer, M.; Ferrero, C.; Diethert, A.; Muller-Buschbaum, P. *J. Appl. Crystallogr.* **2003**, *36*, 684−688.
(19) Fratzl, P.; Jakob, H. F.; Rinnerthaler, S.; Roschger, P.; Klaushofer, K. *J. Appl. Crystallogr.* **1997**, *30*, 765−769.
(20) Paris, O.; Zizak, I.; Lichtenegger, H.; Roschger, P.; Klaushofer, K.; Fratzl, P. *Cell. Mol. Biol.* **2000**, *46*, 993−1004.
(21) Oreski, G.; Wallner, G. M.; Skringer, A.; Pertl, P.; Plessing, A. *EuroSun2004—Proc.* **2004**, *2*, 2-883−2-888.
(22) Lovinger, A. J. In *Development in Crystalline Polymers 1*; Basset, D. C., Ed.; Applied Science: London, 1982; p 195 ff.
(23) Kepler, R. G.; Anderson, R. A. *Adv. Phys.* **1992**, *41*, 1−57.
(24) Lovinger, A. J. *Polymer* **1981**, *22*, 412−413.
(25) Scheinbeim, J. I.; Yoon, C. H.; Pae, K. D.; Newman, B. A. *J. Polym. Sci., Part B: Polym. Phys.* **1980**, *18*, 2271−2276.
(26) Matsushige, K.; Nagata, K.; Imda, S.; Takemura, T. *Polymer* **1979**, *21*, 1391−1397.
(27) Sajkiewics, P.; Wasiak, A.; Goclowski, Z. *Eur. Polym. J.* **1999**, *35*, 423−429.
(28) Castagnet, S.; Gacougnolle, J. L.; Dang, P. *Mater. Sci. Eng., A* **2000**, *276*, 152−159.
(29) Humphreys, J.; Lewis, E. L.; Ward, I. M. *J. Polym. Sci., Part B: Polym. Phys.* **1988**, *26*, 141−158.
(30) Strobl, G. R.; Schneider, M. J. *J. Polym. Sci., Polym. Phys. Ed.* **1980**, *18*, 1343−1359.
(31) Strobl, G. R.; Schneider, M. J.; Voigt-Martin, I. G. *J. Polym. Sci., Polym. Phys. Ed.* **1980**, *18*, 1361−1381.
(32) Guinier, A.; Fournet, G. *Small-Angle Scattering of X-rays*; John Wiley: New York, 1955.
(33) Fratzl, P. *PSI—Proc.* **1997**, *97-01*, 113−128.
(34) Salomons, G. J.; Singh, M. A.; Bardouille, T.; Foran, W. A.; Capel, M. S. *J. Appl. Crystallogr.* **1999**, *32*, 71−81.
(35) Karger-Kocsis, J.; Varga, J. *J. Appl. Polym. Sci.* **1996**, *62*, 291−300.
(36) Rice, J. R. In *Fracture*; Liebowitz, H., Ed.; Academic Press: New York, 1968; Vol. II, pp 191−311.
(37) Rice, J. R.; Johnson, M. A. In *Inelastic Behavior of Solids*; Kanninen, M. F., Ed.; McGraw-Hill: New York, 1970; pp 641−672.
(38) Castagnet, S.; Girault, S.; Gacougnolle, J. L.; Dang, P. *Polymer* **2000**, *41*, 7523−7530.

MA050390F